Synthesis and Electrochemical Properties of Single-Crystal V_2O_5 Nanorod Arrays by Template-Based Electrodeposition

Katsunori Takahashi, Steven J. Limmer, Ying Wang, and Guozhong Cao*

University of Washington, Materials Science and Engineering, 302 Roberts Hall, Box 352120, Seattle, Washington 98195

Received: February 23, 2004; In Final Form: April 28, 2004

This paper reports a study on template-growth and electrochemical properties of single-crystal vanadium pentoxide (V_2O_5) nanorod arrays from $VOSO_4$ aqueous solution using electrochemical deposition. Uniformly sized vanadium oxide nanorods with a length of about 10 μm with diameters ranging from 100 to 200 nm were grown over a large area with near unidirectional alignment. These nanorods have single-crystalline structure with a growth direction of [010]. Electrochemical property analysis indicates that nanorod array electrodes have significantly higher current density and energy storage density than sol−gel-derived V_2O_5 films.

Introduction

In recent years, great attention has been focused on synthesis and applications of nanostructured materials, and one of the most dynamic research areas is on synthesis of one-dimensional nanostructures, such as nanowires, nanorods, and hollow tubes.[1−3] Various techniques have been established and among them, template-based synthesis is one of the most common fabrication methods, particularly for mass production and alignment. Nanorods of numerous materials including metals, polymers, oxides, and composites have been formed using this technique.[4−6] In this method, a porous membrane, such as polycarbonate or anodic alumina, is used as a template and precursor of desired material. Filling of template pores could be achieved by capillary forces,[4] electric field,[6] centrifugation force,[7] and chemical vapor deposition.[8] Electric field has been used for both electrochemical and electrophoretic deposition. Electrochemical deposition, also commonly referred to as electrodeposition, is generally used for the growth of electrically conductive materials, such as metals, semiconductors, and conductive polymers. In this method, electrochemical reactions occur at the electrode−electrolyte interface, and charges are transported through the deposits. In electrophoretic deposition, the electric field induces the oriented migration and stack of charged nanoclusters or nanoparticles on the growth surface, and no electrochemical reactions at the growth surface are required. Therefore, electrophoretic deposition can be used for the growth of dielectric materials. Various dielectric oxide nanorods have been synthesized using a combination of electrophoretic deposition and sol−gel processing.[9,10]

The advantages of template-based growth methods are the ability of fabricating unidirectionally aligned and uniformly sized nanorod arrays of a variety of materials. However, such methods suffer from inherent limitations. In particular, nanorods or nanowires synthesized by template-based growth methods are commonly either amorphous or polycrystalline and porous, which limits further studies on microstructure, properties, and applications of such grown nanorods or nanowires. In addition, post-deposition annealing at elevated temperatures is often required to achieve desired density and mechanical integrity. Poor mechanical integrity and postdeposition annealing often result in break, distortion, and agglomeration of grown nanorods. Further study and development of template-based growth of single-crystal nanorods are obviously of significant importance; however, very limited research has been reported in the literature so far. Martin and co-workers have reported the formation of single-crystal TiO_2 nanorod arrays by filling TiO_2 sol into a polycarbonate membrane with pores of 20 nm in diameter.[11] Miao et al. have grown single-crystal TiO_2 nanorods in a polycarbonate membrane, again with pores of 20 nm in diameter, from a solution.[12] In the latter, localized change of pH as a result of electrolysis reaction of NO_3^- induces the formation of colloidal particles and gelation at the growth surface. No synthesis of single-crystal nanorod arrays of other oxides and/or with diameters larger than 20 nm has been reported using template-based growth methods so far.

Vanadium pentoxide, V_2O_5, has been well studied for various applications. As an intercalation compound, vanadium pentoxide has attracted a lot of attention as an electrode for electrochemical pseudocapacitor applications. When V_2O_5 intercalates Li^+, electrical energy stores in the electrode. Energy releases from the electrode when Li^+ diffuses out. For electrochemical pseudocapacitor applications, the charge/discharge rate and the energy storage capacity are the most important parameters. Larger surface area and easy charge transport are required to achieve high charge/discharge rate.[13,14] V_2O_5 xerogel and aerogel, both offer large surface area, have been explored for such application and have demonstrated a current density of ~6 C (C is about 150 mA h/g V_2O_5) without storage loss. However, V_2O_5 xerogel and aerogels are well-known to suffer from their structural stability; the porous structure readily collapses during Li^+ intercalation and extraction processes. Martin et al.[15] investigated the electrochemical properties of vanadium pentoxide nanorod arrays made by filling vanadium oxide sol into porous polycarbonate membranes, and reported that nanorod arrays achieved a storage capacity of 200 C with small loss and delivered 4 times the capacity of a thin-film electrode (at above 500 C).

In this paper, we investigated (1) the template-growth of single-crystal vanadium pentoxide (V_2O_5) nanorod arrays from

* Corresponding author. E-mail: gzcao@u.washington.edu.

10.1021/jp0491820 CCC: $27.50 © 2004 American Chemical Society
Published on Web 06/15/2004

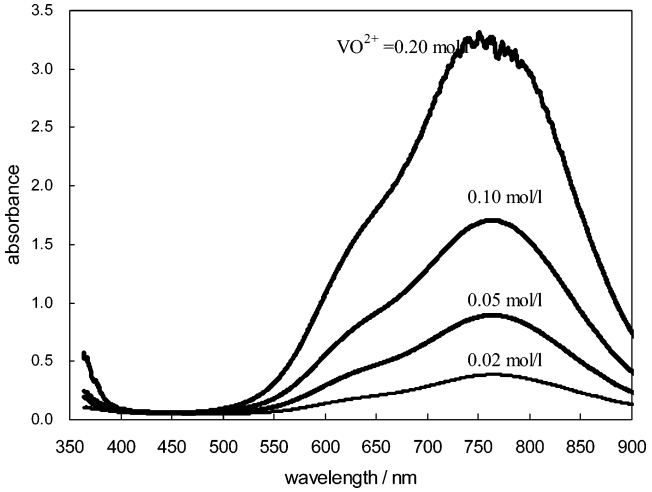

Figure 1. Optical absorption spectra of $VOSO_4$ solution as a function of concentration.

aqueous solution using electrochemical deposition and (2) their electrochemical properties for supercapacitor application. The possible growth mechanisms of single-crystal vanadium oxide nanorod arrays, and the relationship between the electrochemical properties and nanostructures are discussed.

Experimental Section

The chemicals used in making solutions were $VOSO_4 \cdot nH_2O$ (Alfa Aesar) and H_2SO_4 (96.5%, Fisher). A 0.1mol/L VO^{2+} solution was prepared by dissolving $VOSO_4 \cdot nH_2O$ into deionized water together with H_2SO_4 in a molar concentration of 0.1 mol/L. Such a solution has a blue color and a pH of 1.5. In this solution, the primary vanadium ionic clusters are VO^{2+} (vanadium valence of 4+). Solutions with concentration varying between 0.02 mol/L and 0.2 mol/L have been prepared in the same manner. A variation of VO^{2+} concentration in the range of 0.02 mol/L to 0.2 mol/L does not change the valence state of vanadium ions or lead to the formation of new ionic clusters or precipitates as evidenced from the optical absorption spectra shown in Figure 1. Such a solution is stable within a wide range of pH values and vanadium ionic cluster concentration. Nanorod arrays have been grown from this solution inside polycarbonate templates with the assistance of an electric field. The templates used for this study were radiation track-etched hydrophilic PC membrane (Millipore, Bedford, MA) with pore diameters of 200 nm and thickness of 10 μm. For the growth of nanorod arrays, direct electrochemical reactions at the electrolyte and electrode interface are necessary. To ensure a good electrical contact, the backside of the membrane template was first sputter-coated with Au−Pd before attaching to the working electrode. An aluminum sheet 9 mm in diameter was used as the working electrode and placed beneath the template, and Pt mesh was used as a counter electrode. The distance between two electrodes was kept at 25 mm. A detailed description of the deposition setup can be found in our early publications.[9,10] The applied electric voltage ranges from 1.5 V to 2.5 V, and the deposition lasted up to 2 h. Upon the completion of deposition, the samples were dried at 110 °C for 12 h in air, and then fired at 485 °C in air for 1 h to remove the polycarbonate membranes through pyrolysis and oxidation.

Sol−gel-derived vanadia film was also synthesized using a method the same as reported by Fontenot et al.[16] V_2O_5 powder was dissolved in H_2O_2 solution with a V_2O_5 concentration of 0.15 mol/L. HCl was added to keep and preserve VO_2^+ and meta-stable $VO(O_2)(OH_2)^{3+}$. The resulting solution has a H_2O_2/V_2O_5 ratio of 8:1 and HCl/H_2O_2 ratio of 1/10. After stirring for 1.5 h at room temperature, the excess H_2O_2 was decomposed by sonication, and a yellow-brown gel was obtained. The resultant gel was then re-dispersed in deionized water; the resultant sol has a brownish color and contains 0.01mol/L vanadium ion with a pH of 2.7. A sol−gel film was subsequently made by dip coating, followed with firing at 485 °C for 1 h in air. Such a prepared sol−gel film is uniform and crack-free, with a thickness of 1 μm.

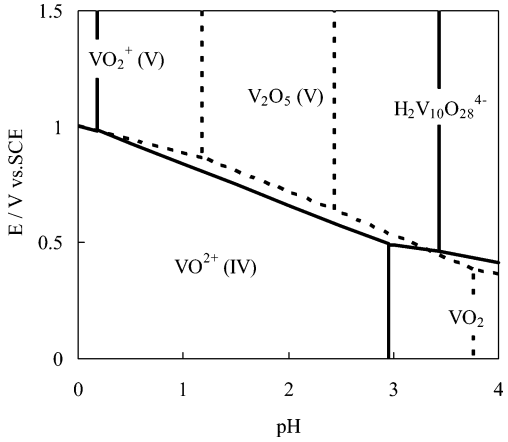

Figure 2. Calculated potential−pH predominant diagram for vanadium oxide species in aqueous solution based on kinetic equilibrium.[18] Solid line shows [V] = 0.1mol/L and dash shows [V] = 0.01mol/L.

Optical absorption spectra of solutions with various concentrations were carried out in the range of 400 nm to 900 nm using a fiber optic spectrometer (Ocean Optics PC2000). Scanning electron microscopy (SEM; JEOL JSM-5200) was used to characterize the morphology of nanorod arrays. Transmission electron microscope (TEM) images and electron diffraction patterns were recorded with Phillips EM420 and JEOL 2010 microscopes at accelerating voltages of 120 kV (Phillips) and 200 kV (JEOL). The crystal structure and crystal orientation of nanorods, gel powders, and films before and after firing were studied by X-ray diffractometry (XRD, Philips PW1830).

Electrochemical properties of nanorod arrays and sol−gel films were investigated using a three-electrode cell. The vanadia nanorod array electrode was made by attaching a PC membrane with grown vanadia nanorods onto an ITO substrate with silver paste, dried first at 110 °C for 8 h, and then heated at 485 °C for 1 h in air to pyrolyze the PC membrane. For the sol−gel film, vanadia sol was directly coated onto ITO substrate and fired at 485 °C in air for 1 h. The apparent surface area of the electrode is 6.4×10^{-5} m^2. A 1 M $LiClO_4$ solution in propylene carbonate is used as electrolyte, and a platinum mesh is used as counter electrode with an $Ag/AgNO_3$ as a reference electrode. Cyclic voltammetry and chronopotentiometric measurements were carried out by a potentiostat/galvanostat (EG&G Princeton Applied Research, model 273).

Results & Discussion

Figure 1 shows the optical absorbance spectra of the VO^{2+} solutions with varied vanadium concentrations. The solution has a broad absorption peak centered around 750 nm with a weak shoulder around 630 nm. Both peaks correspond to the VO^{2+} cluster,[17] which is in a good agreement with the calculated predominance diagram of vanadium species in aqueous solutions (Figure 2).[18] The intensity of these two absorption peaks corresponds very well and increases with an increased vanadium concentration. The peak positions did not change with varied

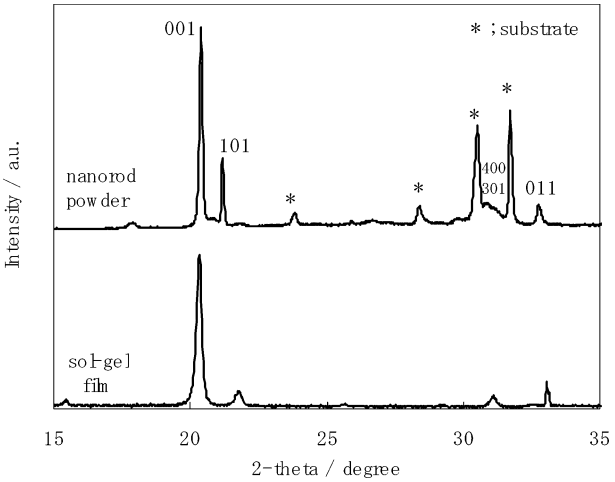

Figure 3. X-ray diffraction patterns of V_2O_5 nanorod powder and sol−gel-derived film.

concentration, and no new peak was found. This observation is indicative that the valence state of vanadium ions was stable in the entire concentration range between 0.02 mol/L and 0.2 mol/L. No chemical reaction took place when the concentration of vanadium varies.

Figure 3 shows X-ray diffraction patterns of the V_2O_5 nanorod powder attached on ITO and V_2O_5 film, both fired at 485 °C for 1 h in air. The XRD spectrum of nanorod array consists of strong (001), (101), and (011) peaks, together with peaks from ITO substrate. Sol−gel-derived V_2O_5 film, obtained by dip coating the colloidal sol onto a substrate followed with annealing, demonstrated strong preferential orientation along the [00*l*] direction. It is well-known in the literature that platelet particles of layer-structured crystalline vanadium oxide form during sol−gel processing and exist in the colloidal sol prior to dip coating. Dip coating will align the platelets parallel on the substrate surface. Annealing at 485 °C is unlikely to change the crystal orientation. However, annealing at 485 °C would effectively densify the sol−gel films, considering the facts of both small particle size and low melting point (T_m = 670; 690 °C)[19,20] of bulk vanadium pentoxide, which is often used as a flux of oxide crystal growth[21] or a sintering aid.[22] The formation of vanadium pentoxide nanorods from VO^{2+} solution is a process significantly different from that of sol−gel-derived film. Growth of nanorods from VO^{2+} solution is a typical electrochemical deposition. At the interface between the electrode (and subsequent growth surface) and electrolyte solution, the ionic cluster, VO^{2+}, is oxidized to deposit solid V_2O_5 through the following reaction:

$$2VO^{2+} + 3H_2O \rightarrow V_2O_5 + 6H^+ + 2e^- \quad (1)$$

A reduction reaction takes place at the counter electrode:

$$2H^+ + 2e^- \rightarrow H_2(g) \quad (2)$$

It is obvious that pH and concentration of VO^{2+} clusters at the vicinity of growth surface shift away from that in the bulk solution; both pH and VO^{2+} concentration decrease. However, the change of pH and VO^{2+} cluster concentration would not lead to the formation of new chemical species as evidenced in Figures 1 and 2. High voltage is likely to lead to a fast growth rate until diffusion becomes a rate-limiting step.

Figure 4 shows a typical SEM image of V_2O_5 nanorod arrays grown from 0.1 mol/L VO^{2+} solution in 200 nm PC membrane under an applied voltage of 1.5 V, and firing at 485 °C for 1 h in air. There is negligible shrinkage along the longitudinal axis and diameters of nanorods. This observation is different from that of the nanorods grown using sol electrophoretic deposition.[9,10] Growth of nanorods by sol electrophoretic deposition is a combination of orientated migration and stack of nanoclusters on growth surface and, therefore, a maximal achievable packing density is ~74% assuming nanoclusters are monosized and spherical. When fired and densified at elevated temperatures, an appreciable shrinkage is expected. However, the vanadium pentoxide nanorods are grown by electrochemical deposition, and the growth species are ionic clusters. Under an appropriate controlled growth condition, fully dense nanorods are expected to deposit inside the template channels.

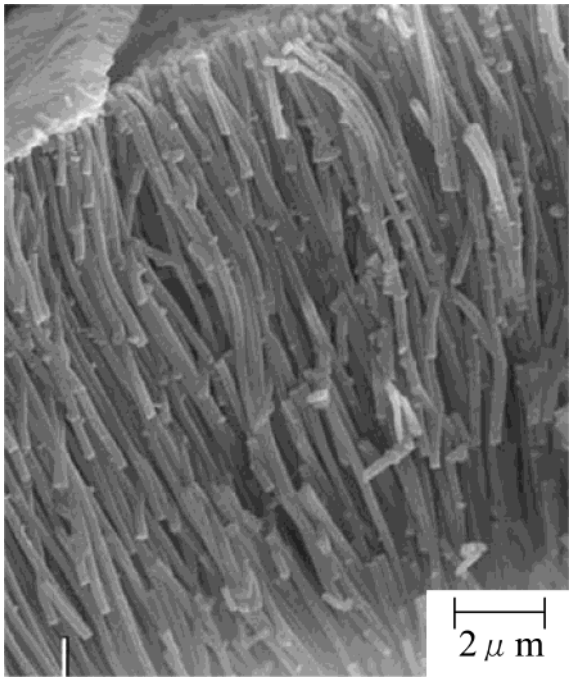

Figure 4. SEM image of V_2O_5 nanorods grown in a PC membrane with 200 nm diameter pores from $VOSO_4$ solution under an applied voltage of 1.5 V after being fired at 485 °C.

Figure 5 shows a TEM micrograph and selected-area electron diffraction pattern of a V_2O_5 nanorod. The diameter of nanorods observed in TEM images is of approximately 50 nm that is much smaller than that found by SEM, which is 150 nm to 200 nm. It is not known to us why such a discrepancy occurs; however, one possible explanation may be attributed to the different sample preparation procedures for SEM and TEM analyses. SEM photographs were taken directly from the nanorods after removal of PC templates by pyrolysis at 485 °C. For TEM, nanorods were mixed with ethanol and subsequently subjected to 15 min sonication for dispersing nanorods. It is possible that sonication may result in delaminating of V_2O_5 sheets and split one nanorod into several smaller nanorods along its axis. Twinning along the growth direction of axis of nanorods may also promote such splitting when subjected to sonication. Of course, it is also possible that one large nanorod as observed in SEM pictures may consist of several smaller single-crystal nanorods as seen in TEM pictures. All these smaller single-crystal nanorods have the same growth direction.

The electron diffraction pattern clearly shows the single-crystalline nature of the nanorod. This pattern can be indexed as orthorhombic V_2O_5 on a [001] zone axis. When the image of the nanorod is overlaid on the diffraction pattern, one observes that the long axis of the nanorod points toward the (020) spot. Thus, if growth occurs along the length of the nanorod, then

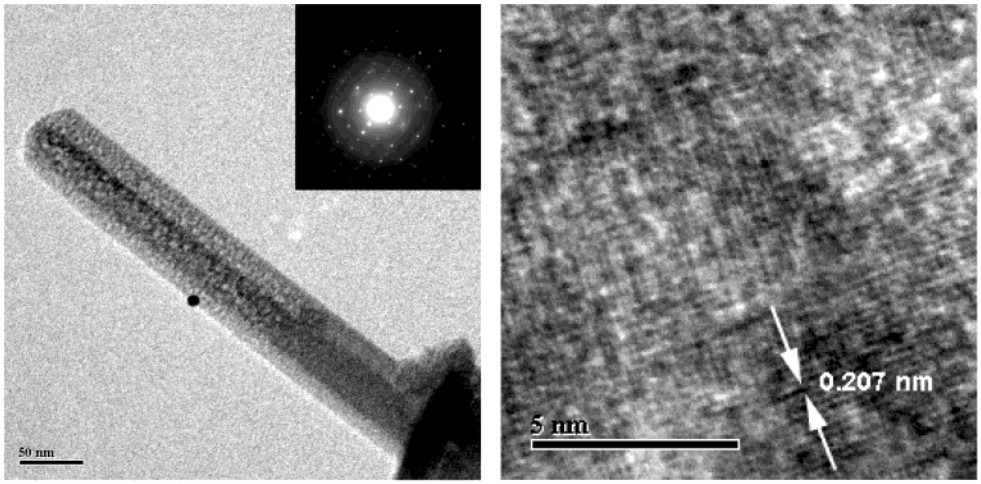

Figure 5. TEM image of a V_2O_5 nanorod grown into a 200 nm membrane and its electron diffraction pattern.

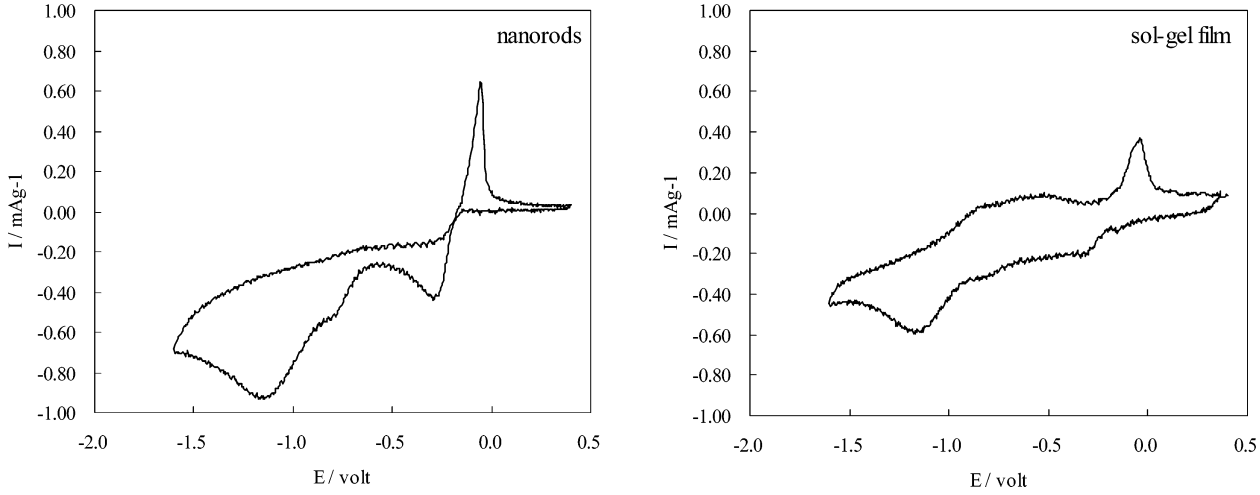

Figure 6. Cyclic voltammograms of V_2O_5 nanorod array (left) and sol−gel-derived film (right) measured using a scan rate of 1 mA/s.

this information suggests a [010] growth direction for the nanorods. Figure 5 also shows a sample high-resolution TEM micrograph of a single V_2O_5 nanorod, in which lattice fringes are clearly visible. The spacing of the fringes was measured to be 0.207 nm, which corresponds well with the spacing of (202) planes at 0.204 nm. These fringes make an angle of 88.9° with the long axis of the nanorod, which is consistent with a growth direction of [010]. Similar measurements made on high-resolution images of other nanorods also yield results consistent with a [010] growth direction. However, these measurements are only consistent with a [010] growth direction; they do not prove that it is the growth direction.

The formation of single-crystal nanorods is attributed to evolution selection growth, which is briefly summarized below. The initial heterogeneous nucleation or deposition on the substrate surface results in the formation of nuclei with random orientation. The subsequent growth of various facets of a nucleus is dependent on the surface energy, and varies significantly from one facet to another.[23] For one-dimensional growth, such as film growth, only the facets with the highest growth rate and perpendicular to the growth surface will be able to continue the growth process. The nuclei with the fastest growth direction perpendicular to the growth surface will grow larger, while slower growth nuclei will eventually cease growth. Such growth results in the formation of columnar-structured films with all the grains having the same crystal orientation (known as textured films).[24] In the case of nanorod growth inside a pore channel,

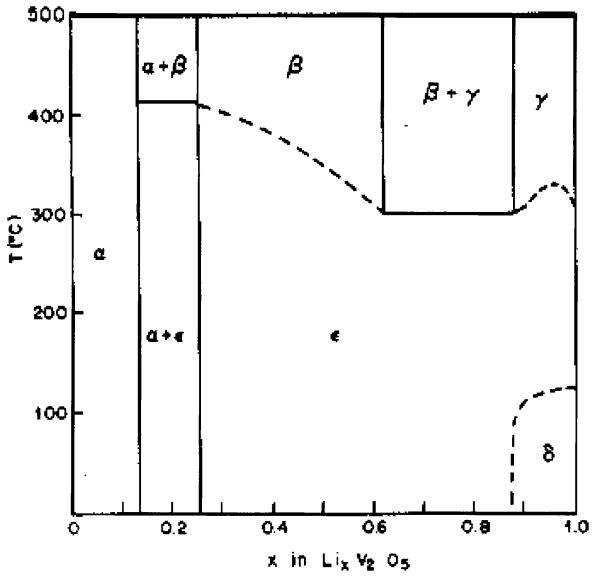

Figure 7. Binary phase diagram of the V_2O_5 −LiV_2O_5 system.[26]

such evolution selection growth is likely to lead to the formation of a single-crystal nanorod. In the case of V_2O_5 crystal, it is well-known that the [010] or *b*-axis is the fastest growth direction, which would explain that single-crystal vanadia nanorods grow along the *b*-axis. It should be noted that such

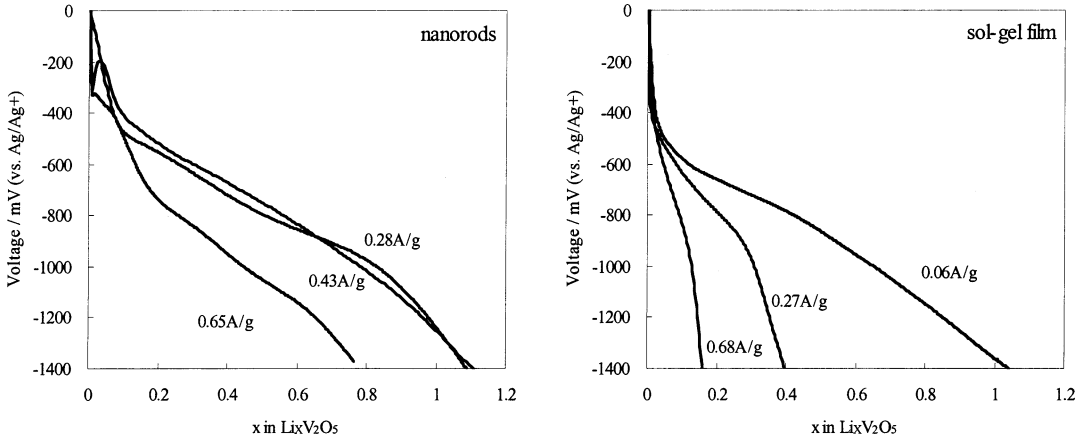

Figure 8. Chronopotentiograms of nanorod arrays (left) and sol−gel-derived films (right) measured with various fixed current density.

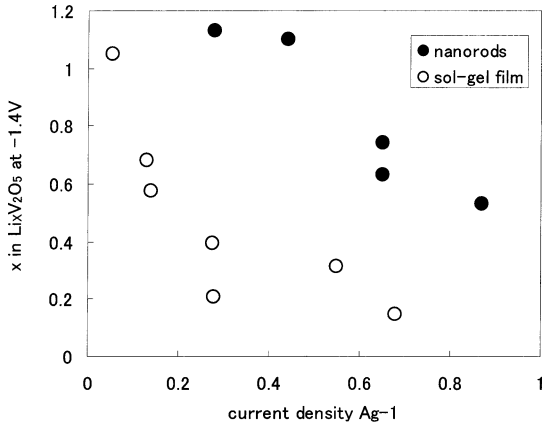

Figure 9. Plot of discharge capacity versus current density for both V_2O_5 nanorod arrays (solid dots) and sol−gel-derived films (empty circles).

evolution selection growth may results in the growth of either one single-crystal nanorod per pore channel or several smaller single-crystal nanorods per pore channel, depending on the initial nucleation. As shown by XRD spectra, sol−gel-derived films have polycrystalline structure with preferential orientation along the [00*l*] axis. Nanorod arrays and films are different in two aspects—single-crystal versus polycrystalline, and (010) versus (001) orientation.

Figure 6 shows typical cyclic voltammograms of V_2O_5 nanorod arrays (left) and sol−gel film (right) measured using a scan rate of 1 mA/s. The cyclic voltammogram of nanorod arrays shows one anodic oxidation peak at 0.0 V, which is attributed to Li^+ extraction, and cathodic peaks at −0.3 V and −1.1 V, which correspond to Li^+ intercalation. For sol−gel films, beside the anodic peak at 0.0 V, another broad anodic peak at −0.7 V is observed. Further, the cathodic peaks at −0.3 and −1.1 V are less distinct. The position of these anodic and cathodic peaks associated with Li^+ extraction and intercalation are well reported in the literature.[25] The integrated area of I−V curves for nanorod array and sol−gel film is identical, which is indicative that both nanorod arrays and films possess the same pseudocapacitance. However, extraction and intercalation kinetics are different as evidenced by the sharp peaks in the nanorod array I−V curve as compared to far less distinctive peaks in the sol−gel I−V curve. For nanorod arrays, there is almost no Li^+ extraction other than at vicinity of 0.0 V with a high discharge current (a sharp tall peak). Such a discharge behavior suggests the nanorod arrays may have no or very little current leakage and a high energy density output. Similarly the cathodic peaks in the nanorod array I−V curve are noticeably better defined; such sharp peaks suggest faster intercalation reactions at given voltages. For the sol−gel film, both charge and discharge peaks are far less well defined and suggest relatively slow extraction and intercalation reaction.

Intercalation and extraction of Li^+ at 0.0, −0.7−0.3, and −1.1 V involve different chemical reactions, resulting in the formation of different phases and can be better understood from the phase diagram of $Li_XV_2O_5$ as shown in Figure 7.[26] $Li_XV_2O_5$ has three different phases at room temperature, which are α ($x < 0.1$), ϵ

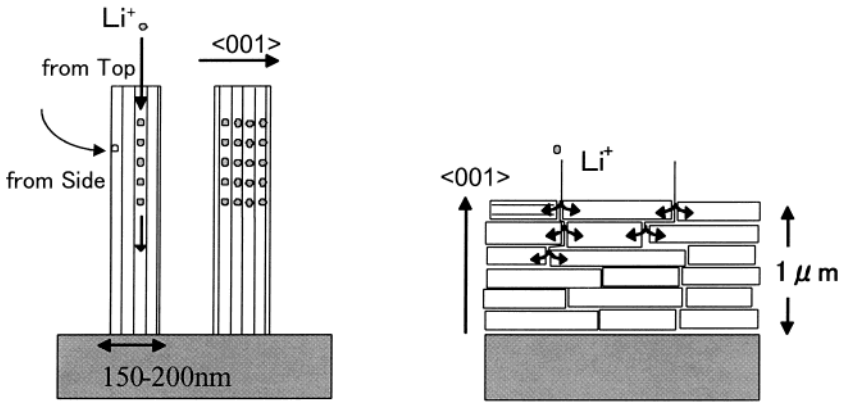

Figure 10. Schematics showing the diffusion paths of Li ions during the intercalation process in both V_2O_5 nanorod arrays (left) and sol−gel-derived films (right). (Scale is not proportional.)

($0.3 < X < 0.8$), and δ ($0.9 < X$) phases. I−V curves suggest that two cathodic peaks correspond to phase changes from α to ϵ, and from ϵ to δ. A broad anodic peak at −0.7 V observed in sol−gel-derived film suggests that a concentration gradient of Li^+ in V_2O_5 crystals exists during the extraction process as reported by Cocciantelli.[27] A nanorod array electrode does not have a peak at −0.7 V, but has one large Li^+ extraction peak at 0.0 V, indicating that nanorod arrays possess minimal Li diffusion resistance.

Figure 8 shows chronopotentiograms of nanorod arrays (left) and sol−gel films (right) for Li^+ intercalation when various fixed current densities were applied. For both nanorod arrays and sol−gel films, lower current densities result in a higher concentration of Li^+ intercalated into vanadium pentoxide electrodes. However, nanorod arrays can intercalate a much higher concentration of Li^+ than that in sol−gel films in a given current density. Sol−gel films can reach the same concentration of Li^+ intercalation only when a significantly lower current density is used. Figure 9 summarizes and compares the current density and Li insertion capacity of nanorod arrays and sol−gel films. In general, for a given Li^+ intercalation capacity, e.g., $Li_{0.7}V_2O_5$, nanorod arrays possess ∼5 times larger current density than that of sol−gel films, and similarly for a given current density, such as 0.7A/g, nanorod arrays can store ∼5 times higher Li than that in sol−gel films.

The differences in electrochemical pseudocapacitor properties observed in vanadium pentoxide nanorod arrays and sol−gels films are attributed to the differences in microstructure and nanostructure of these two different electrodes as schematically illustrated in Figure 10. Vanadia nanorods grown by electrochemical deposition are single crystal, with vanadia layers parallel to the nanorod axis. Such structure is extremely favorable to Li^+ intercalation and extraction, since the surface oxidation and reduction reactions occur along the side surface of nanorods and the solid-state diffusion distance is very small, ∼100 nm, half of the diameter of nanorods. In addition, such structure permits the most freedom for dimension change that accompanies intercalation and extraction reactions. This alignment structure would also enhance the Li^+ diffusion through the solvent. Sol−gel vanadia films are polycrystalline and consist of platelet vanadia grains with [001] perpendicular to the substrate surface. Therefore, the Li^+ intercalation and extraction processes would be comprised of Li^+ diffusion through grain boundaries, oxidation and reduction reactions at the surface of individual crystal grains, and diffusion inside individual grains. The difference in microstructure would have similar effects on the charge transport.

The electrochemical pseudocapacitance of vanadia nanorod arrays observed in the present study is smaller than that reported by Martin and co-workers.[15] Although it is not known why there is such a big difference, the nanorods are different in several aspects. First, the nanorods studied in the paper are single crystalline and 10 μm in length, whereas the nanorods reported in the literature are polycrystalline and 2 μm in length. Second, the 2 μm long polycrystalline nanorods were formed by sol filling, and thus might have a hollow structure (nanotubes), while our nanorods are solid. Furthermore, the polycrystalline nanorods were fired at 400 °C, which may consist of pores, and thus a surface area significantly higher than the apparent surface area. More work is required to clarify and understand this issue.

Conclusions

Single-crystal vanadium pentoxide (V_2O_5) nanorod arrays were grown from $VOSO_4$ aqueous solution by electrochemical deposition using polycarbonate membranes. Uniformly sized vanadium oxide nanorods with a length of about 10 μm with diameters ranging from 100 to 200 nm were grown over a large area with near unidirectional alignment. Nanorods have single-crystalline structures orientated along [010], and the growth of single-crystal vanadium pentoxide nanorods was attributed to an evolution selection growth mechanism. Nanorod array electrodes have approximately 5 times higher applicable current density than sol−gel-derived film, and in a given current density, a nanorod array electrode can intercalate up to 5 times higher concentration of Li^+.

Acknowledgment. A portion of the research described in this paper was performed in the Environmental Molecular Sciences Laboratory, a national scientific user facility sponsored by the Department of Energy's Office of Biological and Environmental Research and located at Pacific Northwest National Laboratory. S.J.L. acknowledges financial support from the NSF-IGERT fellowship from the Center for Nanotechnology at the University of Washington.

References and Notes

(1) Mcllroy, D. N.; Zhang, D.; Kranov, Y.; Norton, M. G. *Appl. Phys. Lett*. **2001**, 79, 1540
(2) Pan, Z. W.; Dai, Z. R.; Wang, Z. L. *Science* **2001**, *291*, 1947
(3) Iijima, S. *Nature* **1991**, *354*, 56.
(4) Martin, C. R. *Science* **1994**, *266*, 1961.
(5) Whitney, T. M.; Jiang, J. S.; Searson, P. C.; Chien, C. L. *Science* **1993**, *261*, 1316.
(6) Huczko, A. *Appl. Phys. A* **2000**, *70*, 365.
(7) Wen, T. L.; Zhang, J.; Chou, T. P.; Limmer, S. J.; Cao, G. Z. Unpublished work.
(8) Kyotani, T.; Tsai, L.; Tomita, A. *Chem. Mater*. **1996**, *8*, 2109.
(9) Limmer, S. J.; Seraji, S.; Forbess, M. J.; Wu, Y.; Chou, T. P.; Nguyen, C.; Cao, G. Z. *Adv. Mater*. **2001**, *13*, 1269.
(10) Limmer, S. J.; Seraji, S.; Forbess, M. J.; Wu, Y.; Chou, T. P.; Nguyen, C. G.; Cao, Z. *Adv. Funct. Mater*. **2002**, *12*, 59.
(11) Lakshimi, B. B.; Patrissi, C. J.; Martin, C. R. *Chem. Mater*. **1997**, *9*, 1544.
(12) Miao, Z.; Xu, D.; Ouyang, J.; Guo, G.; Zhao, X.; Tang, Y. *Nano Lett*. **2002**, *2*, 717.
(13) Watanabe, T.; Ikeda, Y.; Ono, T.; Hibino, M.; Hosoda, M.; Sakai, K.; Kudo, T. *Solid-State Ionics* **2002**, *151*, 313.
(14) Parent, M. J.; Passerini, S.; Owens, B. B.; Smyrl, W. H. *Electrochim. Acta* **1999**, *44*, 2209.
(15) Patrissi, C. J.; Martin, C. R. *J. Electrochem. Soc*. **1999**, *146*, 3176.
(16) Fontenot, C. J.; Wiench, J. W.; Pruski, M.; Schrader, G. L. *J. Phys. Chem. B* **2000**, *104*, 11622
(17) Devi, P. S.; Ganguli, D. *J. Non-Cryst. Solids* **1998**, *240*, 50.
(18) Pourbaix, M. *Atlas of electrochemical equilibria in aqueous solution*; Pergamon Press: New York, 1966; p 234.
(19) International Chemical Safety Cards, No. 0596, 1999.
(20) *CRC Handbook of Chemistry and Physics*, 84th ed.; Lide, D. R., Ed.; CRC Press: Boca Raton, FL, 2003.
(21) Kayama, M.; Kuwano, J. *J. Crystal Growth* **1998**, *193*, 648.
(22) Wu, Y.; Nguyen, C.; Seraji, S.; Forbess, M.; Limmer, S. J.; Chou, T.; Cao, G. Z. *J. Am. Ceram. Soc*. **2001**, *84*, 2882.
(23) van der Drift, A. *Philips Res. Rep*. **1967**, *22*, 267.
(24) Cao, G. Z.; Schermer, J. J.; van Enckevort, W. J. P.; Elst, W. A. L. M.; Giling, L. J. *J. Appl. Phys*. **1996**, *79*, 1357.
(25) Tranchant, A.; Messina, R.; Perichon, J. *J. Electroanal. Chem*. **1980**, *113*, 225.
(26) Murphy, D. W.; Christian, P. A.; Disalvo, F. J.; Waszczak, J. V. *Inorg. Chem*. **1979**, *18*, 2800.
(27) Cocciantelli, J. M.; Menetrier, M.; Delmas, C.; Doumerc, J. P.; Pouchard, M.; Broussely, M.; Labat, J. *Solid State Ionics* **1995**, *78*, 143.